Journal of Colloid and Interface Science 724 (2026) 141222

Contents lists available at ScienceDirect

Journal of Colloid And Interface Science

journal homepage: www.elsevier.com/locate/jcis

Introduction of optimized folate group modification on lipid-coated magnetic nanobeads enables targeting of folate receptor beta

Maximilian Schaaf [a], Svenja Offer [b], Haiyun Zhang [c], Ana Mateos-Maroto [a], Chenxi Li [c], Karl Normak [d], Jacopo Cardellini [d], Lin Jian [a], Kaloian Koynov [a], Manuel Antonio González Gómez [e], Yolanda Piñeiro [e], José Rivas [e], Paolo Arosio [d], Ralf Zimmermann [b,f,j], Andrea Zendrini [d,h], Antonella Bongiovanni [g], Paolo Bergese [g,h,i], Markus Rehberg [c], Katharina Landfester [a], Svenja Morsbach [a,*], Sebastiano Di Bucchianico [b,f]

[a] Department of Physical Chemistry of Polymers, Max Planck Institute for Polymer Research, Mainz 55128, Germany
[b] Comprehensive Molecular Analytics, Helmholtz Center Munich, Neuherberg 85764, Germany
[c] Institute of Lung Health and Immunity (LHI), Comprehensive Pneumology Center (CPC), Helmholtz Center Munich; Member of the German Center for Lung Research (DZL), Munich, Germany
[d] Department of Chemistry and Applied Biosciences, ETH Zurich, Zurich 8093, Switzerland
[e] Department of Applied Physics, Nanomag Group, Materials Institute – iMATUS, Health Research Institute - IDIS, Universidade de Santiago de Compostela-USC, E-15782 Santiago de Compostela, Spain
[f] Department Life, Light & Matter, University of Rostock, Rostock 18059, Germany
[g] IRIB - Institute for Research and Biomedical Innovation of CNR, Palermo, Italy
[h] Department of Molecular and Translational Medicine, Università degli Studi di Brescia, Brescia, Italy
[i] CSGI - Center for Colloid and Interface Science, Firenze, Italy
[j] University of Eastern Finland (UEF), Department of Chemistry and Sustainable Technology/Department of Environmental and Biological Sciences, Joensuu &Kuopio, Finland

HIGHLIGHTS

- Model liposomes were functionalized with folate surface groups via click chemistry.
- Folate density was balanced for good colloidal stability and effective targeting.
- The functionalization strategy was transferred to lipid-coated magnetic nanobeads.
- Folate modified carriers selectively targeted profibrotic M2 macrophages *in vitro*.
- Folate modified carriers targeted macrophages in an *in vivo* lung injury model.

GRAPHICAL ABSTRACT

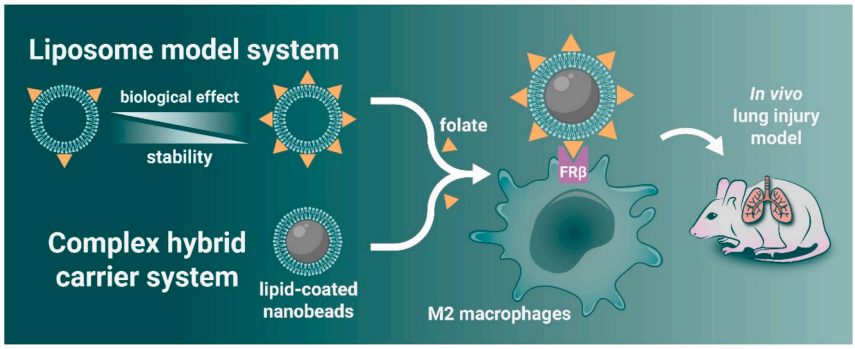

Abbreviation: DBCO, Dibenzocyclooctyne; DLS, Dynamic light scattering; DOPE, 1,2-dioleoyl-*sn*-glycero-3-phosphoethanolamine; FCS, Fluorescence correlation spectroscopy; FRβ, Folate receptor beta; lpMBD, Lipid magnetic bead device; LPS, Lipopolysaccharide; NC, Nanocarrier; NTA, Nanoparticle tracking analysis; PDI, Polydispersity index; SPAAC, Strain-promoted azide-alkyne cycloaddition.

* Corresponding author.
E-mail address: morsbachs@mpip-mainz.mpg.de (S. Morsbach).

https://doi.org/10.1016/j.jcis.2026.141222
Received 25 March 2026; Received in revised form 3 July 2026; Accepted 24 July 2026
Available online 25 July 2026

ARTICLE INFO

Keywords:
Active targeting
Folate receptor beta
Immunomodulation
Nanocarriers
Surface functionalization

ABSTRACT

The functionalization with targeting ligands is a strategy that is often employed to guide nanocarriers to specific target cells. While there is a large variety of different targeting molecules, folate stands out as especially promising. This is because of its high solubility in water, easy experimental handling, and the fact that folate receptor expressing cells present interesting targets for immunomodulation. While folate receptor alpha can be used to target epithelial tumors, folate receptor beta allows targeting of macrophages that are associated to tumors or inflammation sites. However, while several folate-functionalized nanocarriers (NCs) have been reported, studies have almost exclusively focused on targeting outcome, neglecting the effect of folate functionalization on NC colloidal stability. Here, we optimized a two-step functionalization strategy to simultaneously balance both effective targeting and high colloidal stability. Specifically, we optimized the number of functional folate groups depending on overall NC concentration. Here, we observed that high folate group densities required medium NC concentrations, while there was no influence on stability over time. We first validated our strategy using model liposomes and subsequently with a more complex platform consisting of lipid-coated nanobeads (silica-embedded SPIONs), enabling selective targeting and immunomodulation of profibrotic macrophages in relevant *in vitro* and *in vivo* models of lung fibrosis. Folate-functionalized nanocarriers selectively targeted FRβ-expressing M2 macrophages *in vitro* and accumulated in macrophages in a mouse model of lung injury progressing to pulmonary fibrosis whereas unmodified nanocarriers appeared predominantly as isolated particles with no clear cellular association.

1. Introduction

Nanocarriers (NCs) can be functionalized with target-specific ligands to promote their uptake into target cells. Active targeting is a commonly applied method and has resulted in a plethora of highly specific approaches in the nanomedicine field [1–3]. Within targeting ligands, folate stands out as a promising small molecule because of its high specificity, effective cellular uptake, low immunogenicity, and uncomplicated experimental handling due to its simple molecular structure and good water solubility [4]. In human tissue, two types of receptors bind folate: folate receptor alpha (FRα / FOLR1) and folate receptor beta (FRß / FOLR2). FRα is mainly expressed by epithelial cells and is often used as target in epithelial tumors, as found in ovarian, breast, lung, renal, or endometrial cancer. In contrast, FRß is mainly expressed by hematopoietic cells, and facilitates targeting of tumor-associated macrophages or activated macrophages in inflammation, which was shown to be effective for small molecule- or polymer-conjugated folate [5–7].

Lipid-based carriers are well-established in clinical applications, provide easy production and functionalization possibilities, and their composition can be tailored to fit individual requirements [8]. Additionally, lipid membranes are used to coat various types of nanoparticles, such as magnetic nanoparticles for diagnostic or theranostic purposes, thus creating more advanced nanosystems [9]. For specific cell targeting, the surface of lipid-based carriers, such as liposomes, can be functionalized with folate. By introducing functional groups to the lipid head region, they can be covalently linked to targeting moieties such as folate, yielding folate-functionalized nanocarriers. As of today, there are examples of folate-functionalized carriers, varying in composition, functionalization method, and application [10].

However, there is a general lack of quantitative information about the effects of folate functionalization on the colloidal stability of lipid-based NCs [11–13]. Since they are the most widely used NC class in today's clinical applications, it is necessary to understand how reaction and storage conditions and folate density affect the overall NC stability, which is indispensable for a safe use and long shelf-life, while simultaneously providing a biological function in terms of targeting. Additionally, the quantification of relevant functional groups on the lipid NC surface throughout the process is necessary to precisely control reactant ratios and ensure reproducibility. If these requirements are met, folate-functionalization can become available as a tool for a large number of already well-established lipid-based NCs and more advanced systems. Thus, it is ideally suited for applications in the context of lung fibrosis, where it can be employed to target alternatively activated pro-fibrotic macrophages that drive epithelial-to mesenchymal transition, promote fibroblast proliferation, and induce their differentiation into pathogenic myofibroblasts [6,14].

Therefore, we investigated the effect of different folate densities on the physicochemical properties of liposomes, which can be synthesized without limitations regarding sample amount. Then, we transferred this knowledge to *in vitro* and *in vivo* applications of liposome-membrane coated silica-embedded superparamagnetic iron oxide nanoparticles (SPIONS) as depicted in Fig. 1. These hybrids are referred to as so-called "lipid-coated magnetic bead devices") (lpMBDs). Specifically, they effectively combine the biocompatibility of a liposomal membrane with the sophisticated properties of a robust Fe_3O_4 multi-core magnetic nanostructure within a silica shell, which are suited for theranostic applications such as magnetic resonance imaging contrast enhancement, magnetically guided targeting, and magnetic particle hyperthermia [15]. Silica-embedded SPIONS were shown to provide good colloidal stability and biocompatibility [16], rendering them ideal for lipid-membrane coating to create interfaces similar to endogenous membranes on originally inorganic nanoparticles [17].

A click-chemistry based surface functionalization strategy was employed and monitored through functional group quantification assays. After functionalization, the presence of folate was confirmed via fluorescence correlation spectroscopy (FCS) and relevant parameters for reaction control and colloidal stability were readily monitored and reported. After optimization of folate density on liposomes, lpMBDs were folate-functionalized and systematically evaluated in both *in vitro* and *in vivo* settings. *In vitro*, macrophages were differentiated into M0 (low FRß-expressing) and M2 (high FRß-expressing) phenotypes to model resting versus profibrotic macrophage states, enabling a targeted assessment of folate-mediated selectivity. The impact of lpMBDs and folate-lpMBDs on cellular viability, phenotype stability, and inflammatory proteomic profiles was subsequently analyzed to elucidate immunomodulatory effects and underlying molecular mechanisms. Finally, the biodistribution and cellular uptake of lpMBDs and folate-lpMBDs were investigated in an *in vivo* mouse model of acute lung injury progressing to pulmonary fibrosis, demonstrating the translational relevance of this experimental strategy for selectively targeting pathogenic macrophage populations in fibrotic lung disease.

2. Materials and methods

2.1. Synthesis and functionalization

2.1.1. Materials

All chemicals and materials were used as received. Acetone ($\geq$ 99.8% purity) was purchased from VWR (Germany). Ampuwa water was obtained from Fresenius Kabi (Germany). 1,2-Dioleoyl-*sn-glycero*-3-

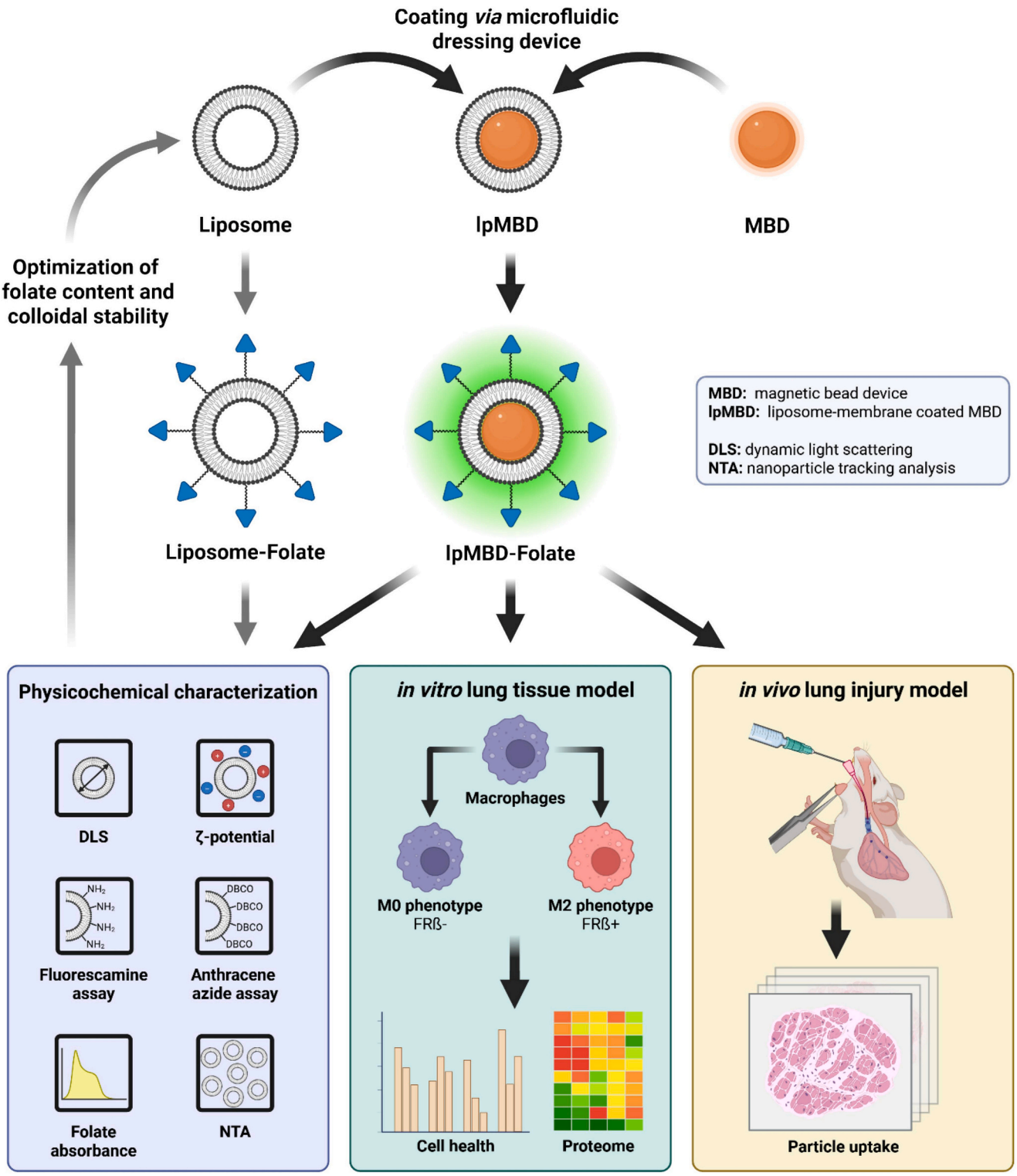

Fig. 1. Schematic summary showing the complete workflow of the study. Magnetic bead devices (MBDs) were coated with liposomal lipid membranes via a microfluidic dressing device [17], yielding liposome-membrane coated MBDs (lpMBDs). lpMBD lipid membranes were labeled with MemGlow™, and the membrane surface was covalently functionalized with folate (lpMBD-folate) to introduce targeting moieties. Physicochemical properties of lpMBD-folate constructs were rigorously characterized and their functionalization strategy optimized regarding folate content and colloidal stability, using representative liposome-folate constructs. Optimized lpMBD-folate were then applied in *in vitro* lung tissue models and *in vivo* lung injury models, yielding immunological data on the cellular and tissue-level and proving the targeting strategy successful. Created in BioRender. Schaaf, M. (2026) https://BioRender.com/bprwi9l

phosphoethanolamine (DOPE, 10 mg mL^{-1}, in chloroform, ≥ 99.0% purity) and L-α-phosphatidylcholine (egg PC, 25 mg mL^{-1}, in chloroform, ≥ 99.0% purity) were procured from Avanti Research (USA). 1,1'-Dioctadecyl-3,3,3′,3′-tetramethylindodicarbocyanine terchlorate (DiD), dimethyl sulfoxide (DMSO, 99.7 + % purity), fluorescamine, and Goat anti-Mouse IgG2b Cross-Adsorbed Secondary Antibody (Alexa Fluor™ 488 labeled) were purchased from Thermo Fisher (Germany). Anti-folic acid antibody (mouse monoclonal), chloroform, cholesterol (Chol), and phosphate buffered saline (PBS, -Mg^{2+}, -Ca^{2+}) (product number D8537) were received from Sigma Aldrich (Germany). DBCO-PEG_4-NHS ester linker was obtained from Jena Bioscience (Germany). Di-sodium tetraborate decahydrate (borax) was procured from Merck Millipore (Germany) and glycine from Carl Roth (Germany). Folate-PEG-azide (HE057006-2 K) was obtained from Biopharma PEG Scientific Inc. (USA). MemGlow™ 488 and MemGlow™ 590 were received from Biozol (Germany). Anthracene azide (Anth-N_3) was synthesized in-house according to a previously published procedure [18]. MBD particles were synthesized according to a procedure described previously [19]. All reagents employed in the synthesis of the magnetic beads devices (MBDs) were used as supplied, with no additional purification steps. Ammonium hydroxide solution (NH_3 aq, 25%), 3-Aminopropyl-triethoxysilane (APTS, 99%), tetraethyl orthosilicate (TEOS, 98%), isopropyl alcohol (IPA, 98%), cyclohexane (CHX, 99.9%) and rhodamine B isothiocyanate (RITC; mixture of isomers) were obtained from MERCK (Saint Louis, MO, USA). Ethanol (absolute grade) was acquired from Panreac (Madrid, Spain). Ultrapure Milli-Q water (Millipore®, Burlington, MA, USA) was used throughout all experimental procedures.

2.1.2. Liposome production and functionalization

2.1.2.1. Liposome production. Liposomes were produced via the lipid film hydration method followed by extrusion through a set of membranes according to a previously published procedure [20]. Briefly, a lipid mixture consisting of L-α-phosphatidylcholine (eggPC), 1,2-dioleoyl-*sn*-glycero-3-phosphoethanolamine (DOPE), and cholesterol (Chol) in the molar ratio of 1:1:1 and a total lipid content of 30 μmol was dissolved in a total of 3.5 mL chloroform in a 50 mL round bottom flask. 30 nmol DiD (26 mM stock solution in DMSO) was added for a final content of 0.1 mol% related to total lipids. In the batch produced for *in vivo* experiments, DiR was added at the same concentration as DiD. The flask was attached to a rotary evaporator and the chloroform was evaporated at 350 mbar, 40 °C, and 150 rpm for 30 min. Residual chloroform was evaporated in a second step at 10 mbar, 40 °C, and 150 rpm for 1 h. The lipid thin film was then hydrated through addition of 4 mL PBS and vortexing until the film was completely detached from the glass. The mixture was stirred with a magnetic stirrer at room temperature (RT) and 500 rpm over-night. Afterwards, the solution was sonicated in a water bath for 20 min at RT and then extruded through polycarbonate membranes to obtain large unilamellar liposomes. The membrane pore sizes were 800 nm, 400 nm, 200 nm, and 100 nm, with eleven extrusions through each membrane. The final liposome solution was stored at 4 °C in the dark until further use.

2.1.2.2. MBD production. Fluorescent MBDs were generated through a tailored reverse microemulsion methodology employing a water-in-cyclohexane system [19]. Before starting the silica shell formation step, RITC was covalently linked to a silane precursor to ensure its incorporation within the silica matrix. Specifically, RITC (0.037 mmol) was reacted with APTS (150 μL) in deoxygenated ethanol (35 mL) and stirred for 16 h in the dark. The resulting RITC–APTS conjugate was stored at 4 °C until further use.

For core–shell assembly, oleic-acid-stabilized Fe_3O_4 nanoparticles (10 mg dispersed in CHX) were added to a mixture of Igepal CO-520 (3.6 mmol) and CHX (18.7 mL), forming a stable reverse microemulsion. Then, NH_3 aq solution (210 μL) initiated the hydrolysis and condensation of TEOS, which was introduced in three sequential portions. The TEOS additions were spaced by 2 h and 1 h, and the reaction was then allowed to proceed for an additional 16 h at room temperature to complete silica deposition around the magnetic cores. The resulting MBDs were isolated by isopropanol-induced precipitation, collected with a NdFeB magnet, and washed repeatedly with isopropanol and water. Finally, the purified MBDs were re-dispersed in Milli-Q water for storage and subsequent experiments.

2.1.2.3. lpMBD production. Liposomes were prepared by dissolving DOPE, POPC, and cholesterol (1:1:1 M ratio) in chloroform. After solvent evaporation under a nitrogen stream, the resulting lipid film was dried under vacuum and rehydrated with Milli-Q water to yield a lipid concentration of 2.5 mg mL^{-1}. The suspension was vortexed to form multilamellar vesicles, which were subsequently subjected to ten freeze–thaw cycles and extruded twenty times through 100 nm pore-size polycarbonate membranes (Whatman, USA) to obtain uniform unilamellar vesicles (ULVs). Coating of MBD particles [19] with liposomes was achieved using a micro-sonication device (μSonicator), as described previously [17]. The μSonicator comprises four piezoelectric transducers attached to a circular glass capillary; applying an alternating electric field drives their vibration, generating a focused acoustic field inside the capillary. For coating, 100 μL of DOPE/POPC/Chol liposomes (2×10^{12} particles mL^{-1}) were mixed with 100 μL of MBD (4×10^{11} particles mL^{-1}) and processed in the μSonicator at a flow rate of 10 μL min^{-1}. An alternating signal of 55 Vpp at 2 MHz (AFG-2225, GW Instek) amplified by a high-frequency amplifier (High Wave 3.2, Digitum-Elektronik) was used to induce the acoustic field.

2.1.2.4. Fluorescent labelling of lipid membranes. Fluorescent labelling of lipid membranes was conducted after liposome or lpMBD formation, using a 20 μM stock solution of MemGlow™ 488 or MemGlow™ 590 fluorogenic membrane probe in DMSO. 1 μL of stock solution per 10^{12} particles was added liposome or lpMBD solution, vortexed briefly and incubated for 15 min with shaking in the dark. Excess dye was removed by centrifugation in pre-wetted Amicon filters (10 kDa MWCO) at RT and 4000 g for 30 min. The supernatant was recovered by inverting the filter into a fresh tube and centrifugation at RT and 4000 *g* for 10 min. PBS was added to reconstitute the supernatant to the volume before washing.

2.1.2.5. Quantification of primary amine groups on the surface of liposomes (Fluorescamine assay). To quantify the primary amines on the liposomes'surface, primary amine groups were derivatized through addition of fluorescamine, followed by fluorescence readout. Standard solutions containing 1 mM, 0.7 mM, 0.5 mM, 0.2 mM, 0.1 mM, 0.05 mM, or 0 mM glycine were used to establish a calibration curve for primary amine concentration. In a 1.5 mL Eppendorf tube, 725 μL borate buffer (0.1 M, pH 9.5) was added to 25 μL standard or sample solution. 250 μL fluorescamine solution (0.3 mg mL^{-1}, in acetone) were added, followed by vortexing at maximum speed for 30 s. After that, 100 μL of the mix was pipetted immediately into three wells of a black, clear bottom 96 well-plate. The fluorescence signal was recorded at 25 °C via a plate reader, with λ_{Ex} = 410 nm and λ_{Em} = 470 nm. Each sample was measured at 0.5×, 0.25×, or 0.125× concentration, and in technical triplicates. Only concentrations that showed values within the linear range of the glycine standard were considered and their deducted values for 1× concentration were averaged.

2.1.2.6. Liposome surface functionalization with DBCO-PEG_4-NHS ester linker. Primary amines on the liposomal surface were subsequently functionalized with DBCO-PEG_4-NHS ester linker at a molar ratio of 0.75:1 (DBCO:NH_2). Considering the primary amine concentration that was determined via fluorescamine assay, linker stock solution (61.57 mM, in DMSO) was added to the fluorescently labeled liposome or

lpMBD solution, followed by brief vortexing and incubation at RT and 500 RPM in a thermoshaker for 2 h in the dark. To remove excess linker, the DBCO-liposome solution was subjected to three washing steps. Each washing step consisted of centrifugation in pre-wetted Amicon filters (100 kDa MWCO) at RT and 3000 g for 1 h. After discarding the flow-through, the supernatant was filled up to 500 µL with PBS. After completing the third washing step, the supernatant was recovered by inverting the filter into a fresh tube and centrifugation at RT and 3000 *g* for 10 min. Recovered supernatants were pooled, and PBS was added to reach the initial volume of DBCO-liposome solution.

2.1.2.7. Quantification of DBCO groups on the surface of liposomes (Anthracene azide assay). To quantify the amount of DBCO groups on the liposomal surface, an anthracene azide (Anth-N_3) assay was performed according to a previously published procedure [18]. An Anth-N_3 stock solution (1.7 mg mL^{-1}, in DMSO) was prepared immediately before the assay and covered with aluminum foil. The following sub-samples were prepared: (a, b) 32.6 µL DMSO +17.3 µL Anth-N_3 stock solution, (c, d) 7.63 µL DMSO +17.3 µL Anth-N_3 stock solution +25 µL liposome sample, (e) 25 µL DMSO +25 µL liposome sample. All samples were vortexed, covered with aluminum foil, and incubated on a stirring plate at RT and 300 rpm over-night. On the following day, each sub-sample (a-e) was used to prepare 100 µL of a 10× and a 100× dilution in DMSO. Each of those diluted sub-samples was transferred to a black, clear bottom 96 well-plate. The fluorescence signal was recorded at 25 °C via a plate reader, with λ_{Ex} = 370 nm and λ_{Em} = 414 nm. The measurement data was processed according to a previously described procedure [21].

2.1.2.8. Particle surface functionalization with folate

2.1.2.8.1. Folate functionalization optimization with liposomes. To optimize the folate-per-particle ratio, five different ratios (0.1:1, 0.25:1, 0.5:1, 0.75:1, and 1:1 (folate:DBCO)) were prepared at a particle concentration of $7*10^{12}$ particles per mL for time stability analysis. Also, three different ratios (0.1:1, 0.5:1, and 1:1 (folate:DBCO)) were prepared at different particle concentrations (6*10 [12], 3*10 [12], 6*10 [11], 3*10 [11], or $6*10^{10}$ particles per mL) for particle concentration stability analysis. Based on the particle concentration and the results from Anth-N_3 assay, the required folate-N_3 stock solution volumes were calculated:

2.1.2.8.2. Folate functionalization of lpMBD. DBCO surface-functionalized lpMBD constructs were functionalized with 0.5 equivalents of folate-per-DBCO.

In 1.5 mL Eppendorf tubes, the liposome solutions were mixed with the respective folate-N_3 stock solution volumes shown in Table 2, pipetted up and down, and incubated at RT and 500 RPM for 18 h in the dark. To remove excess folate-N_3, the solution was subjected to three washing steps. Each washing step consisted of centrifugation in pre-wetted Amicon filters (10 kDa MWCO) at RT and 3000 xg for 1 h. The supernatant was recovered by inverting the filter into a fresh tube and centrifugation at RT and 3000 x*g* for 10 min. PBS was added to the supernatant to reach the initial volume of DBCO-liposome or DBCO-lpMBD solution. Samples were stored at 4 °C in the dark until further use.

2.2. Physicochemical characterization

2.2.1. Solid content and estimation of liposome concentration

To determine the solid content of unfunctionalized liposome solutions, the solvent was evaporated and dry mass was determined relative to a PBS blank. To estimate liposome concentration based on average hydrodynamic diameter and solid content, calculations were performed as previously described by Mateos-Maroto et al. [20]

2.2.2. Dynamic light scattering (DLS)

The hydrodynamic diameter distribution and polydispersity index (PDI) of liposome solutions were measured at 25 °C in a total volume of 200 µL (10 µL sample + 190 µL PBS), using a Zetasizer Nano S90 (Malvern Panalytical GmbH, Germany). Reported values are the mean of *Z*-average values of the main peaks of three technical replicates ± standard deviation.

2.2.3. Zeta potential

Zeta potential of liposome solutions was measured at 25 °C in a total volume of 800 µL (10 µL sample + 790 µL 0.1 M KCl), using a Zetasizer Nano Z (Malvern Panalytical GmbH, Germany). Zeta potential values were calculated as averages and standard deviation of the main peaks of three technical replicates.

2.2.4. Nanoparticle tracking analysis (NTA)

Nanoparticle tracking analysis was used to determine liposome concentration in solution for liposomes used for *in vivo* experiments. Particles were measured using a ZetaView Nanoparticle Tracking Analyzer PMX-230 (TWIN) (Particle Metrix, Germany). Samples were diluted 20,000×, 50,000×, or 100,000× before measurement. Data were analyzed using the ZetaView software (version 8.05.16 SP3). Particle movement was recorded in scatter mode with 1 cycle at 11 positions, at 25 °C.

2.2.5. Folate absorbance

Folate absorbance measurements were conducted via a plate reader, where absorbance of 100 µL sample was recorded at 350 nm and 25 °C.

2.2.6. Fluorescence correlation spectroscopy (FCS)

FCS experiments were performed using a commercial confocal microscope, LSM 880 (Carl Zeiss, Jena, Germany) equipped with a C-Apochromat 40×/1.2 W (Carl Zeiss, Jena, Germany) water immersion objective. An Argon-Ion laser (λ = 488 nm) coupled to the LSM 880 were used for the excitation of the Alexa Fluor 488-labeled secondary antibodies. The emission light at 500–553 nm was detected using a spectral detection unit (Quasar, Carl Zeiss). For each sample, 200 µL of the solution was added to the 8-well polystyrene-chambered cover glass (Nunc Lab-Tek, Thermo Fisher Scientific, Waltham, MA). The confocal detection volume was positioned 90 µm above the glass coverslip, and a series of 20 measurements, 10 s each, were performed at room temperature (23 °C). The obtained experimental autocorrelation curves were fitted with the following analytical model function:

$$G(\tau) = 1 + \left[1 + \frac{f_T}{1 - f_T} e^{-\tau/\tau_T}\right] \frac{1}{N} \sum_{i=1}^{m} \frac{f_i}{\left(1 + \frac{\tau}{\tau_{D,i}}\right) \bullet \sqrt{1 + \frac{\tau}{S^2 \bullet \tau_{D,i}}}} \quad (1)$$

whereby f_T and τ_T are the fraction and the decay time of the triplet state, N is the average number of diffusing fluorescence species in the observation volume, τ_{Di} is the diffusion time of the i-th type of species, f_i is the brightness-weighted number fraction of component i ($1 \le i \le m$), and S is the structure parameter, $S = z_0/r_0$, where z_0 and r_0 represent the axial and radial dimensions of the observation volume. The fits were done using the ZEN 3.0 software (Carl Zeiss, Jena, Germany), which yielded the values of τ_{Di}, N, and S. The diffusion coefficients of the species D_i are related to the respective diffusion times τ_{Di} and the radial dimension r_0 of V_{obs} by $D_i = r_0^2/(4\tau_{Di})$. By inserting D_i into the Stokes-Einstein equation, hydrodynamic radius can be calculated as $R_h = \frac{k_B \bullet T}{6 \bullet \pi \bullet \eta \bullet D}$, here, k_B is the Boltzmann constant, T is the temperature, and η is the viscosity of the solvent. The average fluorescence intensity per molecule(particle), can be calculated as $\frac{<I>}{N}$, where $<I>$ is the average fluorescence intensity. For solutions containing only labeled secondary antibodies, single component (m = 1) fits were applied. For the mixture of secondary antibodies and primary antibodies, and mixture of secondary antibodies, primary antibodies and liposomes, 2 and 3 components model were used, respectively, with the diffusion time of the first component fixed to the value measured for the secondary antibody alone.

The calibration of the confocal volume V_{obs} in each channel was performed by independent FCS experiments with reference dyes with known diffusion coefficients, namely Alexa Fluor 488.

2.3. In vitro exposures

2.3.1. Cell culture, endotoxin assessment and treatments

Human monocytic THP-1 cells (TIB-202, ATCC) were cultured in Roswell Park Memorial Institute medium (RPMI 1640; Gibco, Cat# 21875034, ThermoFisher Scientific) supplemented with 10% sterile-filtered fetal bovine serum (FBS; Sigma-Aldrich Cat# F7524). To differentiate THP-1 monocytes into M0 macrophages, cells were incubated with 250 nM Phorbol-12-myristate-13-acetate (PMA; Sigma-Aldrich, Cat# 524400) in complete medium for 24 h, followed by a 24 h recovery period in PMA-free RPMI medium. Polarization into M2 macrophages was achieved by incubating M0 macrophages for 72 h with 20 ng mL^{-1} each of recombinant human interleukin-4 (IL-4; R&D Systems, Cat# 204-IL) and interleukin-13 (IL-13, R&D Systems, Cat# 213-ILB), as described by Genin and co-authors [22]. Endotoxin levels in different dilutions of liposome formulations, plain liposomes (Lipo), liposomes with folate (Lipo-Folate), and both folate-functionalized (lpMBD-folate) and non-functionalized particles (lpMBD), were assessed using the Pierce Chromogenic Endotoxin Quantification Kit (ThermoFisher Scientific, Cat# A39552), following the manufacturer's instructions. None of the samples showed endotoxin levels higher than 0.1 EU mL^{-1}. M0 and M2 macrophages were exposed to lpMBD-folate or non-functionalized lpMBD particles for either 4 or 24 h in serum-free RPMI 1640 media. Exposures were conducted at varying particle concentrations: 1.5*10 [6], 7.5*10 [6], and 15*10^6 particles mL^{-1}.

2.3.2. Cell viability and cytotoxicity

Cell viability and cytotoxicity were assessed following treatments by evaluating metabolic activity and lactate dehydrogenase (LDH) release, respectively. LDH release into the culture medium served as an indicator of plasma membrane damage. After exposures, conditioned media were collected, and LDH levels were quantified using the Cytotoxicity Detection Kit^{PLUS} (Sigma-Aldrich, Cat# 4744926001) according to the manufacturer's instructions. As positive control, untreated M0 and M2 macrophages were incubated with 0.2% (*v*/v) Triton-X (Sigma-Aldrich, Cat# T8787) to induce maximal LDH release, which was defined as 100% cytotoxicity. Following media collection for LDH analysis, the cells were washed with Dulbecco's phosphate-buffered saline without calcium and magnesium (DPBS, Gibco, Cat# 14190094, ThermoFisher Scientific), and the conditioned media was replaced by RPMI 1640 complete media containing 15% v/v of CellTiter-Blue reagent (Promega, Cat# G8080). After a 1 h incubation at 37 °C in 5% CO_2 atmosphere, fluorescence of the resorufin product ($\lambda_{Ex} = 565$ nm; $\lambda_{Em} = 590$ nm) was measured using a Varioskan LUX microplate reader (ThermoFisher Scientific) equipped with SkanIt Software for Microplate Readers, version 4.1.0.43 (Thermo Fisher Scientific).

2.3.3. Proximity extension assay

Inflammation-related proteins released into the cell culture media were quantified after 4 h and 24 h of treatments of M0 and M2 macrophages with the highest particle concentration (15 * 10^6 particles mL^{-1}). Media samples were analyzed using proximity extension assay (PEA) technology with the Olink Target 96 Inflammation and Immune Response panels (Olink Proteomics AB, Uppsala, Sweden; analysis performed at Proteomics Service Core Facility of the Helmholtz Center Munich, Germany) for a total of 184 unique proteins. Protein levels were expressed as normalized protein expression (NPX) values. Fold changes (FC) relative to untreated M0 and M2 controls were calculated on a log2 scale, and proteins with a log2FC > 0.26 or < -0.26 and a *p*-value < 0.05 were considered differentially expressed (DEP). Downstream analysis of canonical pathways and networks was performed using QIAGEN's Ingenuity Pathway Analysis (IPA, Qiagen) software.

2.4. In vivo exposures

2.4.1. Mice

Female C57BL/6 wild-type mice (Charles River, Sulzfeld, Germany) were maintained under specific pathogen-free conditions at the Helmholtz Zentrum Munich. Animals were housed in individually ventilated cages within a double-barrier facility, supplied with filtered air, and kept on a 12 h light/dark rhythm. Sterilized chow and water were provided ad libitum. Experiments were conducted with mice aged 10–16 weeks, in accordance with regulations of the Upper Bavarian State Government (Regierung von Oberbayern).

2.4.2. Folate-functionalized (lpMBD-folate) or non-functionalized (lpMBD) exposure

Mice were deeply anesthetized by intraperitoneal injection of ketamine/xylazine in saline solution and placed supine on a slanted board. The tongue was gently extended with a forceps and the neck skin illuminated to visualize the epiglottis. A 20-G catheter was carefully introduced into the trachea and correct placement was verified with a defined precision instrument. The intubated mouse was then placed flat on an injection platform and 0.1 μg LPS in 50 μL sterile PBS buffer was administered via a 1 mL syringe with 200 μL volume. Then mice were maintained on warming plates until full recovery from anaesthesia. 20 h later, mice were anesthetized deeply by intraperitoneal injection of a medetomidine–midazolam–fentanyl (MMF) mixture and 7.5 * 10^9 particles (MemGlow™ 590 labeled) or 5 * 10^{10} particles of MemGlow™ 488 labeled particles were instilled intratracheally as described above. After instillation, mice were given 250 μL of antagonist subcutaneously to reverse anaesthesia and support recovery. 4 h after the second instillation, mice were sacrificed with a lethal dose of ketamine/xylazine for subsequent analysis.

2.4.3. Immunofluorescence staining

Frozen lung sections were washed 3 times with DPBS and subsequently blocked with DPBS containing 5% normal goat serum and 0.3% Triton X-100 for 1 h at RT. Sections were then incubated with DAPI (1:1000 dilution in blocking buffer) for 1 h at RT. After staining, slides were washed twice with DPBS containing 0.1% Tween®20 and once with DPBS buffer (5 min each). Finally, sections were mounted with fluorescence mounting medium (Dako Omnis, Agilent, Santa Clara, USA) and covered with glass coverslips.

3. Results and discussion

3.1. Setup of liposome functionalization and validation by physicochemical characterization

To study the influence of folate functionalization on the colloidal stability of lipid-based nanocarriers and optimize reaction conditions, liposomes composed of eggPC, DOPE, and cholesterol (Chol) (1:1:1 M ratio) were produced. The composition is well-established, yields good control over the liposome formation process and provides primary amine groups, which are available for surface functionalization [20,21,23]. Based on a previously published procedure [10], an optimized strain-promoted azide-alkyne cycloaddition (SPAAC) was used to attach azidated folate to the liposomal surface. This approach is very flexible as it can be performed after nanocarrier synthesis with basically any primary amine-containing surface under physiologically-compatible conditions.

Liposomal functionalization with folate was conducted through a two-step process, shown in Fig. 2A. First, the primary amines of DOPE lipids were functionalized with a short PEG-based linker carrying a dibenzocyclooctyne (DBCO)-group. Secondly, folate-PEG-azide was covalently attached via click reaction. Throughout the functionalization process, relevant functional groups were quantified before and after linker conjugation to precisely control reactant ratios. 0.75 equivalents

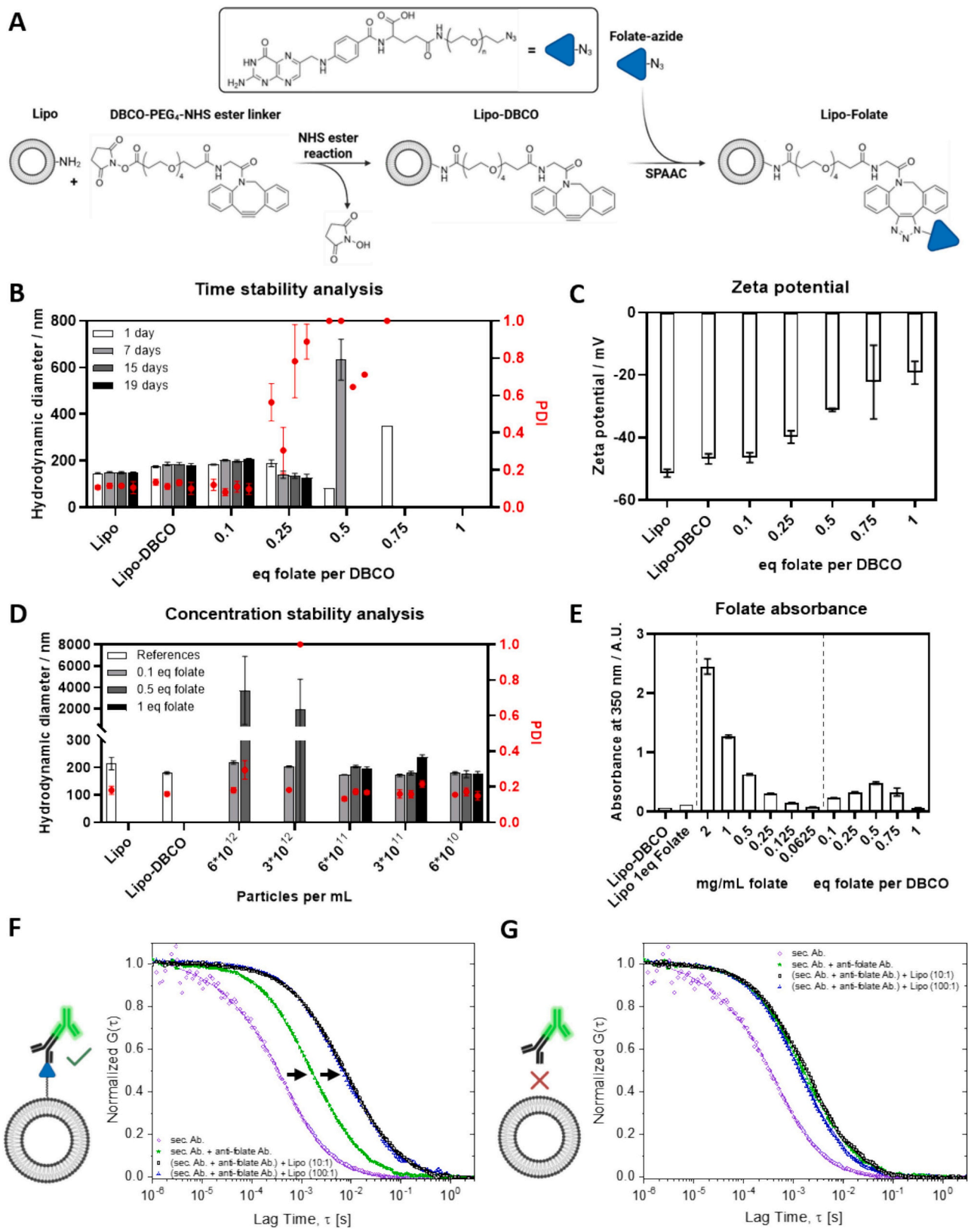

Fig. 2. Liposome functionalization with folate and physicochemical characterization. (A) Schematic summary of the liposome functionalization strategy via strain-promoted azide-alkyne click chemistry (SPAAC). (B) Time stability analysis of liposome constructs via DLS before and after folate functionalization for varied folate per DBCO group ratios (at $7*10^{12}$ particles per mL). (C) Zeta potential analysis of liposome constructs before and after folate functionalization. (D) Concentration stability analysis of liposome constructs via DLS before and after folate functionalization. (E) Folate absorbance of folate standard solutions and liposome constructs before and after folate functionalization. For (B–E), Values are the mean of three technical replicates ± standard deviation. Normalized FCS autocorrelation curves recorded for solutions of fluorescently labeled secondary antibodies, non-labeled primary anti-folate antibodies and either folate functionalized (F) or non-factionalized (G) liposomes. Created in BioRender. Schaaf, M. (2026) https://BioRender.com/bprwi9l

(eq) of DBCO-linker per primary amine on DOPE (DBCO:NH_2) was identified as an ideal ratio to provide sufficient functionalization sites without influencing colloidal stability (Fig. S1). Higher DBCO:NH_2 ratios did not increase the number of converted NH_2 groups significantly. Therefore, this parameter was fixed in all following experiments. Various folate-per-DBCO (folate:DBCO) equivalents were tested at varying liposome concentrations, and colloidal stability was monitored through dynamic light scattering (DLS) and zeta potential measurements. Fig. 2B summarizes the hydrodynamic diameter (D_h) and polydispersity index (PDI) of liposomes functionalized with 0.1, 0.25, 0.5, 0.75, or 1 eq folate:DBCO, over the course of up to 19 days. The zeta potential of the same set of samples was measured after one day, shown in Fig. 2C. To account for the effect of liposome/nanocarrier concentration on the colloidal stability of the system, liposomes were diluted to particle concentrations ranging from $6*10^{12}$ to $6*10^{10}$ liposomes per mL and subsequently functionalized with 0.1, 0.5, or 1 eq folate:DBCO. The respective D_h and PDI values are summarized in Fig. 2D, while representative size distributions are shown in Fig. S2. To connect the findings from DLS and zeta potential to the concentration of folate in each sample, folate absorbance measurements at 350 nm were conducted. Results are shown in Fig. 2E.

The range of 0.1–1 eq folate:DBCO was chosen to provide a balance between folate-receptor targeting and colloidal stability. On the one hand, studies have shown that higher folate densities on the nanocarrier surface are beneficial for targeting folate receptors [24], especially when targeting FRα [25]. On the other hand, folate conjugation can lead to a more neutral zeta potential by shielding the lipid head group charges and thus decrease the nanocarrier's colloidal stability through less electrostatic repulsion [26]. Indeed, we observed that at a high liposome concentration, increasing the folate density led to a less negative zeta potential (Fig. 2C) and decreased colloidal stability (Fig. 2B) at pH 7.4. Probably, the rather bulky net neutral folate group screens the remaining negative charge of the DOPE phosphate group. This reduced stability could also be observed by folate absorbance, where higher folate:DBCO ratios led to increased folate detection from 0.1 eq to 0.5 eq folate:DBCO (Fig. 2E), followed by a decreased folate detection towards 1 eq folate:DBCO, which is most likely caused by aggregation and material loss during washing steps. Interestingly, we found that this negative effect on colloidal stability could be partially compensated by decreasing the liposome concentration, allowing for higher folate densities at lower liposome concentrations (Fig. 2D). While at concentrations $\geq 3*10^{12}$ liposomes per mL, only 0.1 eq folate yielded colloidally stable folate-functionalized liposomes, concentrations $\leq 6*10^{11}$ liposomes per mL allowed for up to 1 eq folate without impeding colloidal stability. This is most likely caused by the decreased number of liposome-liposome encounters in a less crowded solution, decreasing the probability of aggregation events [27]. We concluded that folate density and liposome concentration are the two main parameters that determine the colloidal stability of folate-conjugated liposomes, with storage times up to 19 days showing no observable effect. For the planned transfer of functionalization to lpMBDs, their particle concentration was taken into account as well. As they were usually obtained in a range of 10^{11} to 10^{12} particles per mL (Table 1), we considered the use of 0.5 eq folate to be ideal to provide a balance between high folate load and colloidal stability. Although at $6*10^{11}$ liposomes per mL, 1 eq folate did not result in aggregation, the more neutral zeta potential was considered a risk factor for a complex particle system like lpMBDs. Van der Waals attractions of MBD cores together with a high folate density could increase the propensity for aggregation. On this basis, 0.5 eq folate were chosen over 1 eq.

Finally, fluorescence correlation spectroscopy (FCS) was used to confirm the presence of accessible folate on the liposomal surface. The FCS technique is somewhat similar to DLS as it also measures hydrodynamic radius, but in contrast to DLS it monitors only fluorescent (or labeled) species. Thus, it is particularly suitable for studying the interactions between small fluorescent antibodies and larger non fluorescent liposomes [28]. To enable FCS, folate-functionalized or non-functionalized liposomes were incubated with 10 or 100 equivalents antibodies:liposomes of a primary anti-folate antibody and a secondary fluorescently labeled antibody. These equivalents were chosen since the expected number of folate molecules per liposome was within the range of tens to hundreds. After incubation, the mixtures were analyzed via FCS. Fig. 2F shows the FCS autocorrelation curves recorded for folate-functionalized liposomes and values obtained from the fitting are summarized in Table S1. The curve recorded for solutions containing only fluorescently labeled secondary antibody (green), yielded a value of 9 ± 1 nm for the hydrodynamic radius (R_h), which is in line with the reported hydrodynamic radius of an antibody in solution [29,30]. Upon mixing with primary antibody, R_h increased to 64 ± 6 nm, and the average fluorescence intensity per particle increased ~9-fold, indicating the formation of large multimers through antibody–antibody interactions. Finally, the addition of folate-functionalized liposomes led to a further stark increase in R_h (black and blue) ($R_h = 223 \pm 22$ nm for 10 eq., $R_h = 292 \pm 29$ nm for 100 eq.), indicating binding of the primary folate antibody and secondary antibody to the folate on the liposomal surface. The average fluorescence intensity per liposome increased ~3-fold from 10 eq. to 100 eq., suggesting that a higher antibody-to-liposome ratio led to more primary and, consequently, secondary antibodies being attached to the liposomes.

As a negative control, non-functionalized liposomes were incubated

Table 2
Folate-N_3 stock solution volumes required for lpMBD functionalization.

Fluorescent label	Sample	DBCO per mL	Volume (μL)	Folate-N_3 stock solution Volume (μL)
MemGlow™ 488	Lipo-linker	$5.6*10^{14}$	100	5.8 (8 μM)
	lpMBD-linker	$8.1*10^{14}$	400	33.8 (8 μM)
MemGlow™ 590	Lipo-linker	$4.4*10^{16}$	300	13.8 (0.8 mM)
	lpMBD-linker	$3.3*10^{16}$ ‡	300	10.4 (0.8 mM)

‡ Due to repeated problems with this sample in the Anth-N_3 assay, this value was calculated by multiplying the value received for the Lipo-Linker with the ratio of the primary amine concentration of both samples, assuming the degree of linker functionalization to be the same.

Table 1
Folate-N_3 stock solution volumes required for liposome functionalization.

Particles per mL	DBCO per mL	Volume (μL)	Folate-N_3 stock solution (0.8 mM) volume (μL) For a folate: DBCO ratio of				
			0.1:1	0.25:1	0.5:1	0.75:1	1:1
$7*10^{12}$	$2.2*10^{17}$	400	18	45	89	134	179
$6*10^{12}$	$3.0*10^{17}$	500	31.7		158.3		316.6
$3*10^{12}$	$1.5*10^{17}$	500	15.8		79.2		158.3
$6*10^{11}$	$3.0*10^{16}$	500	3.2		15.8		31.7
$3*10^{11}$	$1.5*10^{16}$	500	1.6		7.9		15.8
$6*10^{10}$	$3.0*10^{15}$	500	0.3		1.6		3.2

Table 3
DLS, NTA, and zeta potential analysis of MemGlow™ –labeled liposome and lpMBD samples before and after folate functionalization. D_h and zeta potential values were calculated as averages and standard deviation of the main peaks of three technical replicates. PDI and particles per mL values were calculated as averages and standard deviation of three technical replicates.

Batch	Sample	DLS		NTA	Zeta potential
		D_h/ nm	PDI	Particles per mL	mV
MemGlow™ 488 labeled	Lipo	129 ± 1	0.177 ± 0.017	(2.8 ± 0.3) *10^{12}	–
	lpMBD	311 ± 4	0.261 ± 0.017	(1.9 ± 0.1) *10^{11}	–
	Lipo-folate	115 ± 1	0.077 ± 0.005	(4.0 ± 0.6) *10^{11}	–
	lpMBD-folate	325 ± 11	0.312 ± 0.011	(2.4 ± 0.3) *10^{11}	–
MemGlow™ 590 labeled	Lipo	141 ± 5	0.122 ± 0.029	(1.8 ± 0.3) *10^{12}	−14 ± 4
	lpMBD	272 ± 8	0.102 ± 0.030	(6.5 ± 0.7) *10^{11}	−21 ± 2
	Lipo-folate	170 ± 9	0.156 ± 0.003	(4.4 ± 0.4) *10^{11}	−31 ± 1
	lpMBD-folate	280 ± 14	0.270 ± 0.010	(1.5 ± 0.2) *10^{11}	−24 ± 15

with the same set of antibodies. The respective FCS autocorrelation curves are shown in Fig. 2G. Here, while the addition of primary antibody led to an increase in secondary antibody size (purple to green) as before, further addition of non-functionalized liposomes did not lead to another size increase (black and blue). This indicates that no anti-folate antibody could bind to the liposomes, in the absence of folate.

In summary, FCS studies could qualitatively confirm the presence of accessible folate molecules on the liposomal surface.

3.2. lpMBD functionalization and physicochemical characterization

After studying the parameters influencing colloidal stability of folate-functionalized liposomes, the complexity of the system was increased by advancing from liposomes to lpMBDs, which were previously developed to enhance the performance of nanomaterials like MBDs in biological applications [17]. Basic characterization of the applied magnetic beads (MBDs) is shown in Table S2, Fig. S3-S4 and in previous publications [19,31]. To enable tracking of lpMBDs *in vitro* and *in vivo*, their lipid membrane (DOPE:POPC:Chol, 1:1:1) was labeled using MemGlow™ 488 or 590. The choice of dye was made as it enables post-production labelling, which might prevent loss of dye during hybrid formation, and allows future replacement of the synthetic lipid membrane with biological ones such as extracellular vesicles. For the lpMBD formation, the lipid composition of applied liposomes was slightly refined. To provide more control over the hybrid formation process, POPC was used instead of eggPC. POPC is composed of the fatty acids C16:0 and C18:1, which are the main components of eggPC as well – however eggPC contains a small amount of additional fatty acids differing slightly in chain length. This was found to ensure reliable coating of MBDs with lipid membranes without influencing the folate functionalization procedure at all. Consequently, the same functionalization strategy as used for liposomes was applied, using 0.5 eq folate: DBCO. With an average of roughly 500 DBCO moieties per particle and the high yield of SPAAC reactions, 0.5 eq folate:DBCO can result in up to ~250 folate groups per nanocarrier. This value is within the range of a medium ligand density, which is known to be advantageous for targeting [32,33]. The physicochemical characterization of the resulting MemGlow™-labeled and folate-functionalized lpMBD samples is summarized in Table 3, including DLS, NTA, and zeta potential data. Representative size distribution curves are shown in Fig. S5.

D_h and PDI were not significantly altered by liposome and lpMBD folate conjugation, indicating that the applied functionalization procedure did not impair colloidal stability and optimization of the functionalization procedure with the liposomal model system was successful in terms of transferring the process to lpMBDs. Compared to liposomes, lpMBD hybrids generally showed increased D_h and PDI values as reported in Table 3. This is, however, not a sign for poor lpMBD stability, but rather a reflection of their intrinsic heterogeneity as previously reported by Cardellini et al. [17]

3.3. Biological evaluation in vitro

To assess exposure-dependent cellular responses and to establish the *in vitro* safety, selectivity, and immunomodulatory potential of the nanocarriers, increasing concentrations of lpMBD or lpMBD-folate particles were applied *in vitro* to macrophages for 4 h and 24 h. Experiments were performed on nonactivated M0 monocyte-derived macrophages, which exhibit low FRβ expression (Fig. 3A), and on anti-inflammatory M2 macrophages displaying high FRβ levels (Fig. 3B), to directly evaluate the selectively of folate-functionalized nanocarriers for FRβ-expressing, profibrotic macrophages and to distinguish effects on resting versus pathogenic macrophage phenotypes. Cytotoxicity was evaluated by lactate dehydrogenase (LDH) release from damaged cell membranes, cell viability was assessed based on cellular reducing activity, and differential immunogenicity was analyzed using affinity-based proteomics.

3.3.1. In vitro cell viability and cytotoxicity

After 4 h of exposure, a dose-dependent increase in cytotoxicity was observed, although it did not reach statistical significance, with no differences between lpMBD and lpMBD-folate in either M0 or M2 macrophages (Fig. 3C). After 24 h, only the highest concentrations of both lpMBD and lpMBD-folate caused a slight increase in membrane damage in M2 macrophages (Fig. 3E). Nonetheless, no significant reduction in metabolic activity was observed at either exposure time or in either macrophage phenotype (Fig. 3D and F). These results indicate that functionalizing lpMBD with folate does not impair naive or alternatively activated macrophages viability and metabolic activity. This is in line with literature reports as it has been demonstrated that the functionalization of polymeric liposome-coated SPIONs with folate did not reduce the viability of HeLa adenocarcinoma epithelial cells when compared to non-functionalized particles [34].

3.3.2. In vitro immunomodulatory capacity

To evaluate the effect of folate-functionalization on macrophage response, we assessed the immunomodulatory properties of lpMBDs with and without surface-attached targeting groups. Distinct effects were observed following both 4 h (Fig. 4A and C) and 24 h (Fig. 4B and D) exposures across treatment conditions and macrophage phenotypes relative to their respective controls. Short term exposures of M0 macrophages to lpMBD-folate particles induced the highest number of unique differentially expressed proteins (DEPs) compared to other treatments and was associated with increased levels of the immunosuppressive protein CD274, chemokine ligands CCL13 and CCL19, the cell surface receptor IL10RA, and cytokines IL18 and IL33. These changes suggest a potential polarization of M0 macrophages towards a M2-like phenotype. However, CD274 was also upregulated after 4 h M0 exposure to lpMBD. Together with the increased expression of CLEC4D and the cell signalling regulator SPRY2, this pattern may also instead reflect a broader M0 macrophage activation response (Fig. 4A and C, Table S3).

An increased number of DEPs was observed after 24 h exposure of M0 macrophages to lpMBD (Fig. 4B and D, Table S3). This treatment upregulated the growth factor TGFB1, the detoxification enzyme SULT1A1, and the chemokine CX3CL1, while downregulating the immunosuppressive glycoprotein CLEC7A. The observed effects may reflect a persistent shift of M0 macrophages towards a regulatory and metabolically adaptive state in response to lpMBD exposure. Both folate-

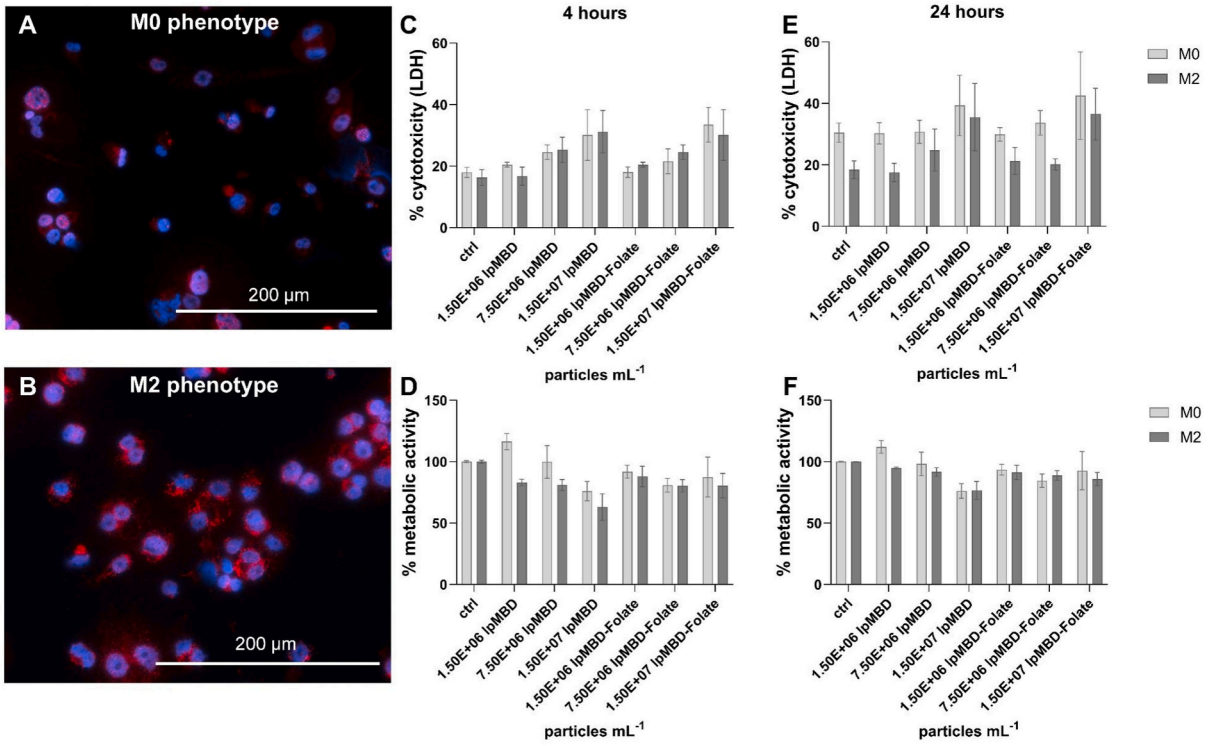

Fig. 3. Folate receptor **β** (FR**β**) immunostaining and cellular health. (A) M0 and (B) M2 polarised THP-1 macrophages; red: FR**β**, blue: DAPI nuclear staining. Cellular health following 4 h (C and D) and 24 h (E and F) M0 or M2 macrophages treatments with increasing concentrations of lpMBD or lpMBD-folate. Cytotoxicity was evaluated as lactate dehydrogenase (LDH) leakage (C and E). Metabolic activity was assessed by evaluating the reducing power of cells (D and F). Data are presented as mean ± standard error of mean from three independent experiments ($n = 3$). (For interpretation of the references to colour in this figure legend, the reader is referred to the web version of this article.)

free and functionalized lpMBDs downregulated the potassium channel regulator DPP10, the cytokine receptor IFNLR1, and the interleukin 1 receptor associated kinase IRAK4. Together, this profile is consistent with a dampened innate immune activation state and aligns with the reduced IL6 secretion observed in M0 macrophages after 24 h of lpMBD exposure.

In M2 macrophages, 24 h exposure to both lpMBD and lpMBD-folate increased the number of DEPs, but with distinct profiles, except for the increased secretion of the endocrine factor FGF21, a major metabolic regulator. Folate-free lpMBDs upregulated anti-apoptotic signalling molecules DFFA, TRAF2, and TANK; the immune modulatory IL15RA, CD40, and IL6, as well as the metabolic and stress-response adaptive proteins ADA, EGLN1, HEXIM1, and PRDX5. Collectively, this profile reflects immunoregulatory activity and enhanced resilience to cellular stress induced by lpMBD. In contrast, lpMBD-folate induced a similar but more pronounced and statistically robust response (Fig. 4B and D) including chemokines and immune cell recruitment proteins CCL25 and CCL28, as well as co-stimulatory and immune modulation proteins CD6, CD8A, and TREM1. This pattern highlights enhanced interactions with T-cells and a stronger M2-specific immunomodulatory signature, consistent with the phenotype's role in inflammation resolution, tissue repair, and homeostasis.

Overall, while the exposure time shaped M0 macrophage immunoregulation, with both lpMBD and lpMBD-folate particles associated with positive PC2 values after 4 h exposure and negative values after 24 h treatments, folate functionalization clearly discriminates M2 macrophage responses, promoting a faster, stronger and more persistent immunomodulatory profile compared to folate-free lpMBD (Fig. 4E).

In conclusion, the data indicate that both exposure time and macrophage phenotype significantly influence protein secretion, with M2 macrophages showing a more pronounced upregulation of reparative and immunomodulatory proteins compared to M0, and that lpMBD-folate treatment further enhances these M2-specific responses relative to folate free lpMBD particles, suggesting a faster and persistent cellular uptake in a biocompatible context which was further investigated in profibrotic mice models.

3.4. *Biological evaluation in vivo*

Finally, *in vivo* lung macrophage targeting of MemGlow™ 488 and MemGlow™ 590 labeled lpMBDs and lpMBD-folate was investigated in a preclinical mouse model of endotoxin (LPS 0.1 µg) induced lung inflammation.

Fluorescence microscopy on lung slices of mice receiving these particles via instillation (4 h) after pre-treatment with LPS (20h) to enhance expression of FRβ [5] showed a stronger fluorescence signal localized in macrophage-like cells for the lpMBD-folate compared to unfunctionalized lpMBDs (Fig. 5A–C). As anticipated, due to reduced tissue autofluorescence in the red imaging channel compared to the green channel, the MemGlow™ 590 label was superior to the MemGlow™ 488 label (Fig. 5A and B). However, in both cases the lpMBD-folate exhibited clear cellular localization, which was not present in lung tissue obtained from unfunctionalized lpMBDs instilled mice.

lpMBD-folate particles accumulated in cells with the morphology and tissue distribution characteristic of macrophages, whereas unmodified lpMBDs appeared as isolated particles without distinct cellular association. This suggests that folate functionalization enhanced macrophage targeting of lpMBDs within the lung tissue. In general, it has to be noted that equal numbers of MemGlow™ 590 labeled particles (lpMBDs, lpMBD-folate) were instilled into the lungs of LPS-pretreated mice. Interestingly, folate modification decreased the observed fluorescence intensity in the lungs. Since equal numbers of particles were administered in all conditions, the observed reduction in fluorescence is likely based on a reduction of fluorescence intensity after the folate

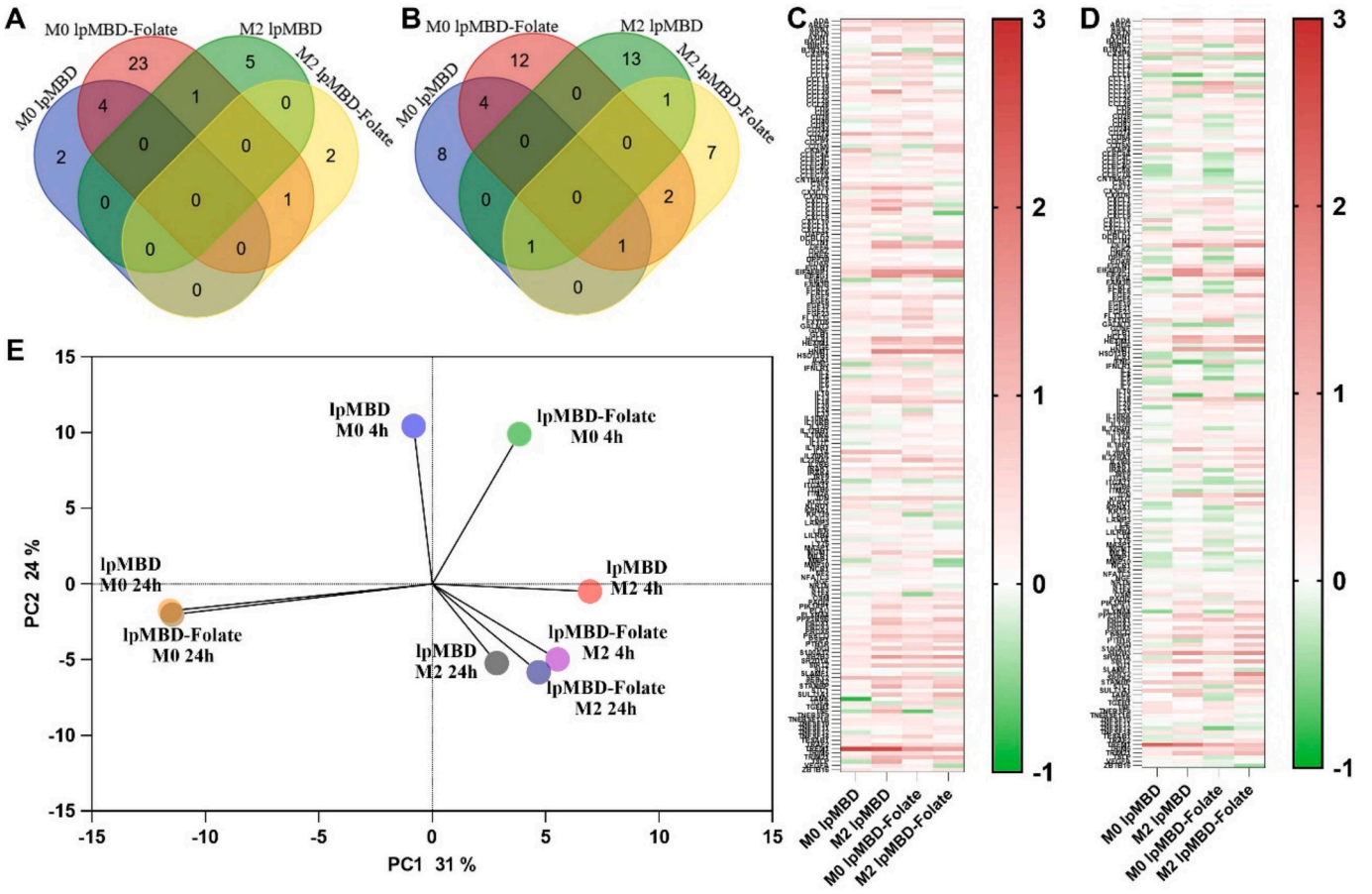

Fig. 4. Proximity extension assay (PEA) analysis of *in vitro* immunomodulation. (A, B) Venn diagrams showing the number of unique and overlapping significant differentially expressed proteins after 4 h (A) and 24 h (B) treatments of M0 or M2 macrophages with the highest concentration of lpMBD or lpMBD-folate. (C, D) Heatmaps showing the overall protein level patterns (log2 fold change) after 4 h (C) and 24 h (D) treatments. (E) Proportion of variance explained by principal components in the analysis of 184 protein levels following exposures of M0 or M2 macrophages to lpMBD or lpMBD-folate.

functionalization process. Although neither folate nor the reagents used for its conjugation are known to act as direct quenchers in the 600–620 nm spectral range, indirect quenching effects cannot be excluded.

Taken together, lpMBD-folate exhibit cellular targeting superior to lpMBD particles and MemGlow™ 590 labeling is ideally suited for detection in the highly autofluorescent lung tissue.

4. Conclusion

In this study, folate was conjugated to liposomes and liposome-coated magnetic bead devices (lpMBDs) to investigate the resulting effects on colloidal stability and interactions with folate receptor beta (FRß)-expressing cells. Through physicochemical analysis, *in vitro* studies with M0 and M2 macrophages, and *in vivo* studies in a mouse model of lung inflammation, folate functionalization was optimized towards high colloidal stability and biological efficacy.

Liposomes were used as a model system to optimize folate functionalization parameters. Tested parameters included DBCO-per-NH_2 ratio, DBCO-per-folate ratio, liposome concentration, and storage time. For that purpose, functional group quantification assays and physicochemical analysis methods including DLS, zeta potential analysis, folate absorbance analysis, and FCS were employed. Insights from the liposomal system were then transferred to the more complex lpMBD system, combining a liposome shell-membrane with a stiff magnetic nanostructure, that yielded colloidally stable, folate functionalized constructs. These were then tested *in vitro* on M0 (low FRß) or M2 (high FRß) macrophages. While no effect on cell viability or metabolic activity was observed, it was found that both exposure time and macrophage phenotype significantly influenced protein secretion. Overall, the strongest upregulation of immunomodulatory proteins was found when M2 macrophages were incubated with lpMBD-folate, indicating a higher and more effective cellular uptake. Finally, constructs were tested *in vivo* within the context of a preclinical mouse model of endotoxin induced lung inflammation. Here, lpMBD-folate showed enhanced cell uptake in macrophage-like cells.

In summary, folate functionalized liposomes and lpMBDs with high colloidal stability were produced, leading to effective targeting of lpMBDs towards FRß-expressing cells *in vitro* and *in vivo*. This was made possible by balancing the number of folate surface groups versus overall nanocarrier concentration, which was found to be essential for the stability of lipid-based nanocarriers. Finally, high colloidal stability combined with sufficient targeting group density enabled the successful application in profibrotic *in vitro* and *in vivo* models.

CRediT authorship contribution statement

Maximilian Schaaf: Writing – review & editing, Writing – original draft, Methodology, Investigation, Formal analysis. **Svenja Offer:** Writing – review & editing, Methodology, Investigation, Formal analysis. **Haiyun Zhang:** Writing – review & editing, Methodology, Investigation, Formal analysis. **Ana Mateos-Maroto:** Methodology, Investigation, Formal analysis. **Chenxi Li:** Methodology, Investigation, Formal analysis. **Karl Normak:** Methodology, Investigation, Formal analysis. **Jacopo Cardellini:** Methodology, Investigation, Formal analysis. **Lin Jian:** Methodology, Investigation, Formal analysis. **Kaloian Koynov:** Methodology, Investigation, Formal analysis. **Manuel**

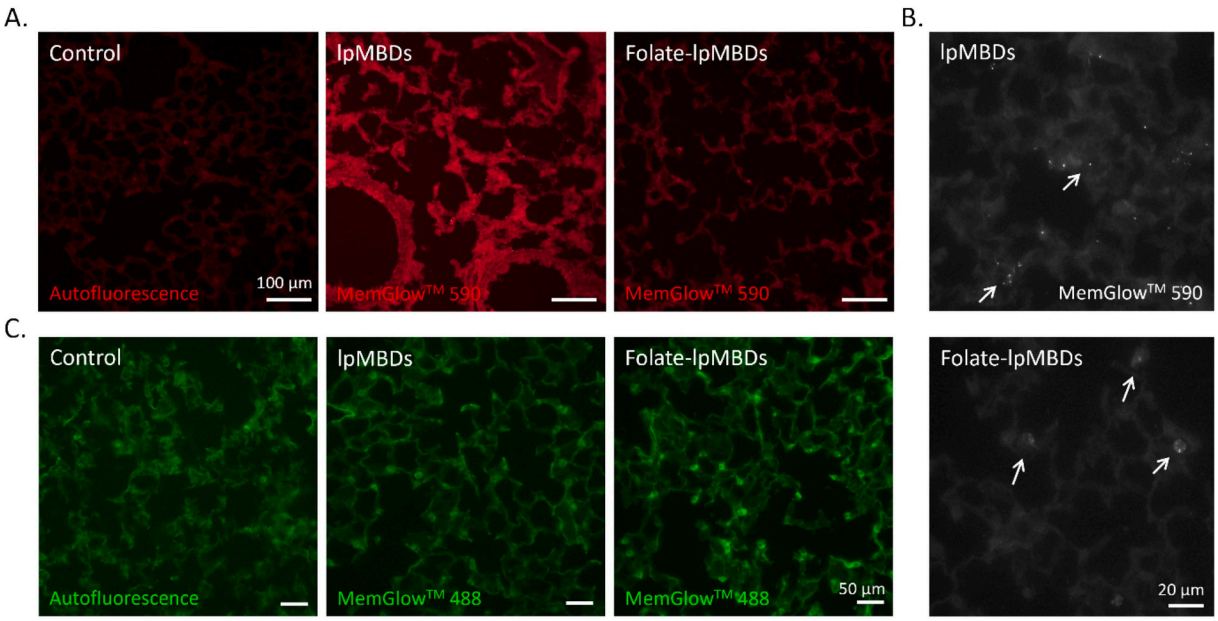

Fig. 5. lpMBD-folate exhibit uptake in pulmonary macrophages. Mice were pretreated by instillation of 0.1 µg LPS (24 h) to induce expression of folate receptor beta (FRβ) on macrophages in the lungs. Thereafter, mice received either 5 * 10^{10} particles of MemGlow™ 488 stained lpMBDs and lpMBD-folate (n = 2 mice per treatment), or 7.5 * 10^{9} particles of MemGlow™ 590 stained lpMBDs, lpMBDs-folate, or vehicle (control) (n = 3 per treatment), via instillation (4 h). (A) Representative fluorescence microscopy images of lung slices from MemGlow™ 590 labeled samples (B) Representative confocal microscopy images of lung slices from MemGlow™ 590 labeled samples. n = 3 mice. (C) Representative fluorescence microscopy images of lung slices from MemGlow™ 488 labeled samples. Note the strong tissue autofluorescence present under control conditions in the green channel, which was almost absent in the red channel depicted in (A).

Antonio González Gómez: Methodology, Investigation, Formal analysis. **Yolanda Piñeiro:** Methodology, Investigation, Formal analysis. **José Rivas:** Writing – review & editing, Resources. **Paolo Arosio:** Writing – review & editing, Resources. **Ralf Zimmermann:** Writing – review & editing, Resources. **Andrea Zendrini:** Writing – review & editing, Project administration. **Antonella Bongiovanni:** Writing – review & editing, Project administration, Conceptualization. **Paolo Bergese:** Writing – review & editing, Project administration, Funding acquisition, Conceptualization. **Markus Rehberg:** Writing – review & editing, Resources, Project administration, Methodology, Conceptualization. **Katharina Landfester:** Writing – review & editing, Resources, Project administration, Funding acquisition, Conceptualization. **Svenja Morsbach:** Writing – review & editing, Supervision, Project administration, Methodology, Conceptualization. **Sebastiano Di Bucchianico:** Writing – review & editing, Visualization, Supervision, Resources, Project administration, Methodology, Funding acquisition, Conceptualization.

Declaration of competing interest

The authors declare the following financial interests/personal relationships which may be considered as potential competing interests: Jose Rivas reports financial support was provided by European Commission. Paolo Arosio reports financial support was provided by European Commission. Antonella Bongiovanni reports financial support was provided by European Commission. Paolo Bergese reports financial support was provided by European Commission. Katharina Landfester reports financial support was provided by European Commission. Sebastiano di Bucchianico reports financial support was provided by European Commission. If there are other authors, they declare that they have no known competing financial interests or personal relationships that could have appeared to influence the work reported in this paper.

Acknowledgments

This work was supported by the BOW (Biogenic Organotropic Wetsuits) project funded by the European Union's Horizon 2020 research and innovation programme, under the grant agreement No 952183. Additionally, we thank Stefan Schuhmacher for graphical assistance.

Appendix A. Supplementary data

Supplementary data to this article can be found online at https://doi.org/10.1016/j.jcis.2026.141222.

Data availability

Data will be made available on request.

References

[1] F. Salahpour Anarjan, Active targeting drug delivery nanocarriers: ligands, Nano Struc. Nano Objects 19 (2019) 100370, https://doi.org/10.1016/j.nanoso.2019.100370.
[2] B. Dutta, K.C. Barick, P.A. Hassan, Recent advances in active targeting of nanomaterials for anticancer drug delivery, Adv. Colloid Interf. Sci. 296 (2021) 102509, https://doi.org/10.1016/j.cis.2021.102509.
[3] W. Yi, P. Xiao, X. Liu, Z. Zhao, X. Sun, J. Wang, L. Zhou, G. Wang, H. Cao, D. Wang, et al., Recent advances in developing active targeting and multi-functional drug delivery systems via bioorthogonal chemistry, Signal Transduct. Target. Ther. 7 (1) (2022) 386, https://doi.org/10.1038/s41392-022-01250-1.
[4] S.A. Kularatne, P.S. Low, Targeting of nanoparticles: folate receptor, in: Cancer Nanotechnology: Methods and Protocols, Springer, 2010, pp. 249–265.
[5] W. Han, R. Zaynagetdinov, F.E. Yull, V.V. Polosukhin, L.A. Gleaves, H. Tanjore, L. R. Young, T.E. Peterson, H.C. Manning, L.S. Prince, et al., Molecular imaging of folate receptor β–positive macrophages during acute lung inflammation, Am. J. Respir. Cell Mol. Biol. 53 (1) (2015) 50–59, https://doi.org/10.1165/rcmb.2014-0289OC (acccessed 3/5/2026).
[6] F. Zhang, E.A. Ayaub, B. Wang, E. Puchulu-Campanella, Y.H. Li, S.U. Hettiarachchi, S.D. Lindeman, Q. Luo, S. Rout, M. Srinivasarao, et al., Reprogramming of profibrotic macrophages for treatment of bleomycin-induced pulmonary fibrosis, EMBO Mol. Med. 12 (8) (2020) EMMM202012034, https://doi.org/10.15252/emmm.202012034.
[7] D.J. O'Shannessy, E.B. Somers, L.C. Wang, H. Wang, R. Hsu, Expression of folate receptors alpha and beta in normal and cancerous gynecologic tissues: correlation of expression of the beta isoform with macrophage markers, J. Ovarian Res. 8 (1) (2015) 29.

[8] G. Bozzuto, A. Molinari, Liposomes as nanomedical devices, Int. J. Nanomedicine (2015) 975–999.
[9] A. Luchini, G. Vitiello, Understanding the nano-bio interfaces: lipid-coatings for inorganic nanoparticles as promising strategy for biomedical applications, Front. Chem. 7 (2019) 343.
[10] P. Sahane, N. Puri, P. Khairnar, V. Phatale, S. Shukla, A. Priyadarshinee, S. Srivastava, Harnessing folate receptors: a comprehensive review on the applications of folate-adorned nanocarriers for the management of melanoma, ACS Appl. Bio Mater. 8 (5) (2025) 3623–3656.
[11] P. Ebrahimnejad, A.S. Taleghani, K. Asare-Addo, A. Nokhodchi, An updated review of folate-functionalized nanocarriers: a promising ligand in cancer, Drug Discov. Today 27 (2) (2022) 471–489.
[12] M. Ahmadi, C.A. Ritter, T. von Woedtke, S. Bekeschus, K. Wende, Package delivered: folate receptor-mediated transporters in cancer therapy and diagnosis, Chem. Sci. 15 (6) (2024) 1966–2006.
[13] M.A.I. Ibrahim, R. Othman, C.F. Chee, F. Ahmad Fisol, Evaluation of folate-functionalized nanoparticle drug delivery systems—effectiveness and concerns, Biomedicines 11 (7) (2023) 2080.
[14] L. Zhang, Y. Wang, G. Wu, W. Xiong, W. Gu, C.-Y. Wang, Macrophages: friend or foe in idiopathic pulmonary fibrosis? Respir. Res. 19 (1) (2018) 170, https://doi.org/10.1186/s12931-018-0864-2.
[15] X. Wang, Y. Wang, Z. Xue, W. Wan, Y. Li, H. Qin, Y. Zhu, F. Tian, J. Yang, Magnetic liposome as a dual-targeting delivery system for idiopathic pulmonary fibrosis treatment, J. Colloid Interface Sci. 636 (2023) 388–400, https://doi.org/10.1016/j.jcis.2023.01.007.
[16] M. Romano, M.A. González Gómez, P. Santonicola, N. Aloi, S. Offer, J. Pantzke, S. Raccosta, V. Longo, A. Surpi, S. Alacqua, et al., Synthesis and characterization of a biocompatible nanoplatform based on silica-embedded SPIONs functionalized with polydopamine, ACS Biomater. Sci. Eng. 9 (1) (2023) 303–317, https://doi.org/10.1021/acsbiomaterials.2c00946.
[17] J. Cardellini, K. Normak, M. Gerlt, K. Makasewicz, C. Seiffert, U. Capasso Palmiero, S. Ye, M.A. González Gómez, Y. Piñero, J. Rivas, Microfluidics-driven manufacturing and multiscale analytical characterization of nanoparticle-vesicle hybrids, Adv. Healthc. Mater. 14 (4) (2025) 2403264.
[18] G. Baier, J.M. Siebert, K. Landfester, A. Musyanovych, Surface click reactions on polymeric nanocapsules for versatile functionalization, Macromolecules 45 (8) (2012) 3419–3427, https://doi.org/10.1021/ma300312n.
[19] P. Garcia Acevedo, M.A. Gonzalez Gomez, A. Arnosa Prieto, L. De Castro Alves, R. Seco Gudina, Y. Piñeiro, J. Rivas, Fluorescent single-core and multi-core nanoprobes as cell trackers and magnetic nanoheaters, Magnetochemistry 8 (8) (2022) 83.
[20] A. Mateos-Maroto, M. Gai, M. Brückner, R. da Costa Marques, I. Harley, J. Simon, V. Mailänder, S. Morsbach, K. Landfester, Systematic modulation of the lipid composition enables the tuning of liposome cellular uptake, Acta Biomater. 158 (2023) 463–474.
[21] M. Gai, J. Simon, I. Lieberwirth, V. Mailänder, S. Morsbach, K. Landfester, A bio-orthogonal functionalization strategy for site-specific coupling of antibodies on vesicle surfaces after self-assembly, Polym. Chem. 11 (2) (2020) 527–540, https://doi.org/10.1039/C9PY01136F.
[22] M. Genin, F. Clement, A. Fattaccioli, M. Raes, C. Michiels, M1 and M2 macrophages derived from THP-1 cells differentially modulate the response of cancer cells to etoposide, BMC Cancer 15 (1) (2015) 577.
[23] A. Mateos-Maroto, M. Gai, M. Brückner, V. Mailänder, S. Morsbach, K. Landfester, Controlled functionalization strategy of proteins preserves their structural integrity while binding to nanocarriers, Adv. Mater. Interfaces 11 (30) (2024) 2400472, https://doi.org/10.1002/admi.202400472.
[24] Z. Tang, D. Li, H. Sun, X. Guo, Y. Chen, S. Zhou, Quantitative control of active targeting of nanocarriers to tumor cells through optimization of folate ligand density, Biomaterials 35 (27) (2014) 8015–8027, https://doi.org/10.1016/j.biomaterials.2014.05.091.
[25] S.K. Jones, A. Sarkar, D.P. Feldmann, P. Hoffmann, O.M. Merkel, Revisiting the value of competition assays in folate receptor-mediated drug delivery, Biomaterials 138 (2017) 35–45.
[26] D. Lombardo, M.A. Kiselev, Methods of liposomes preparation: formation and control factors of versatile nanocarriers for biomedical and nanomedicine application, Pharmaceutics 14 (3) (2022) 543.
[27] X. Xu, F. Tian, Y. Pan, T. Zhang, L. Deng, H. Jiang, J. Han, J. Liu, Y. Zhao, W. Liu, Emerging mechanistic insights into liposomal stability: full process management from production and storage to food application, Chem. Eng. J. 505 (2025) 159552.
[28] S. Schmitt, L. Nuhn, M. Barz, H.J. Butt, K. Koynov, Shining light on polymeric drug nanocarriers with fluorescence correlation spectroscopy, Macromol. Rapid Commun. 43 (12) (2022) 2100892.
[29] P. Gagnon, R. Nian, D. Leong, A. Hoi, Transient conformational modification of immunoglobulin G during purification by protein a affinity chromatography, J. Chromatogr. A 1395 (2015) 136–142, https://doi.org/10.1016/j.chroma.2015.03.080.
[30] C.G. Conner, J. McAndrew, S. Menegatti, O.D. Velev, An accelerated antibody aggregation test based on time sequenced dynamic light scattering, Colloids Surf. A Physicochem. Eng. Asp. 653 (2022) 129833, https://doi.org/10.1016/j.colsurfa.2022.129833.
[31] M.A. González-Gómez, Á. Arnosa-Prieto, P. García-Acevedo, P. Diaz-Rodriguez, L. de Castro-Alves, Y. Piñeiro, J. Rivas, Surface-modified iron oxide nanoprobes in biomedical scaffolds, Nanoscale Adv. 7 (24) (2025) 8093–8103, https://doi.org/10.1039/D5NA00605H.
[32] D.R. Elias, A. Poloukhtine, V. Popik, A. Tsourkas, Effect of ligand density, receptor density, and nanoparticle size on cell targeting, Nanomedicine 9 (2) (2013) 194–201.
[33] K. Schorr, S. Beck, O. Zimmer, F. Baumann, M. Keller, R. Witzgall, A. Goepferich, The quantity of ligand–receptor interactions between nanoparticles and target cells, Nanoscale Horiz. 10 (4) (2025) 803–823.
[34] Z. Liao, H. Wang, R. Lv, P. Zhao, X. Sun, S. Wang, W. Su, R. Niu, J. Chang, Polymeric liposomes-coated superparamagnetic iron oxide nanoparticles as contrast agent for targeted magnetic resonance imaging of cancer cells, Langmuir 27 (6) (2011) 3100–3105.